nature physics

Article

https://doi.org/10.1038/s41567-024-02708-5

Thermally driven quantum refrigerator autonomously resets a superconducting qubit

Received: 3 June 2023

Accepted: 11 October 2024

Published online: 9 January 2025

Check for updates

Mohammed Ali Aamir [1] ✉, Paul Jamet Suria [1], José Antonio Marín Guzmán [2], Claudia Castillo-Moreno [1], Jeffrey M. Epstein[2,3], Nicole Yunger Halpern [2,3] ✉ & Simone Gasparinetti [1] ✉

Although classical thermal machines power industries and modern living, quantum thermal engines have yet to prove their utility. Here, we demonstrate a useful quantum absorption refrigerator formed from superconducting circuits. We use it to cool a transmon qubit to a temperature lower than that achievable with any one available bath, thereby resetting the qubit to an initial state suitable for quantum computing. The process is driven by a thermal gradient and is autonomous, requiring no external feedback. The refrigerator exploits an engineered three-body interaction between the target qubit and two auxiliary qudits. Each auxiliary qudit is coupled to a physical heat bath, realized with a microwave waveguide populated with synthesized quasithermal radiation. If the target qubit is initially fully excited, its effective temperature reaches a steady-state level of approximately 22 mK, lower than what can be achieved by existing state-of-the-art reset protocols. Our results demonstrate that superconducting circuits with propagating thermal fields can be used to experimentally explore quantum thermodynamics and apply it to quantum information-processing tasks.

Quantum thermodynamics should be more useful. The field has yielded fundamental insights, such as extensions of the second law of thermodynamics to small, coherent and far-from-equilibrium systems[1–8]. Additionally, quantum phenomena have been shown to enhance engines[9–12], batteries[13] and refrigerators[14]. These results are progressing gradually from theory to proof-of-principle experiments. However, quantum thermal technologies remain experimental curiosities, not practical everyday tools. Key challenges include control[15] and cooling quantum thermal machines to temperatures that support quantum phenomena. Both challenges require substantial energy and effort but yield small returns. For example, one would expect a single-atom engine to perform only about an electronvolt of work[16].

Autonomous quantum machines offer hope. First, they operate without external control. Second, they run on heat drawn from thermal baths, which are naturally abundant[17]. A quantum thermal machine would be useful in a context that met three criteria. (1) The machine fulfils a need. (2) The machine can access real-world different-temperature baths. (3) No or few extra resources are spent on maintaining whatever coherence is necessary for the machine's operation.

We identify such a context: qubit reset. Consider a superconducting quantum computer starting a calculation. The computer requires qubits initialized to their ground states[18]. If left to thermalize with its environment as thoroughly as possible, though, a qubit could achieve only an excited-state population of ~0.01–0.03, or an effective

[1]Department of Microtechnology and Nanoscience, Chalmers University of Technology, Gothenburg, Sweden. [2]Joint Center for Quantum Information and Computer Science, NIST and University of Maryland, College Park, MD, USA. [3]Institute for Physical Science and Technology, University of Maryland, College Park, MD, USA. ✉e-mail: aamir.ali@chalmers.se; nicoleyh@umd.edu; simoneg@chalmers.se

https://doi.org/10.1038/s41567-024-02708-5

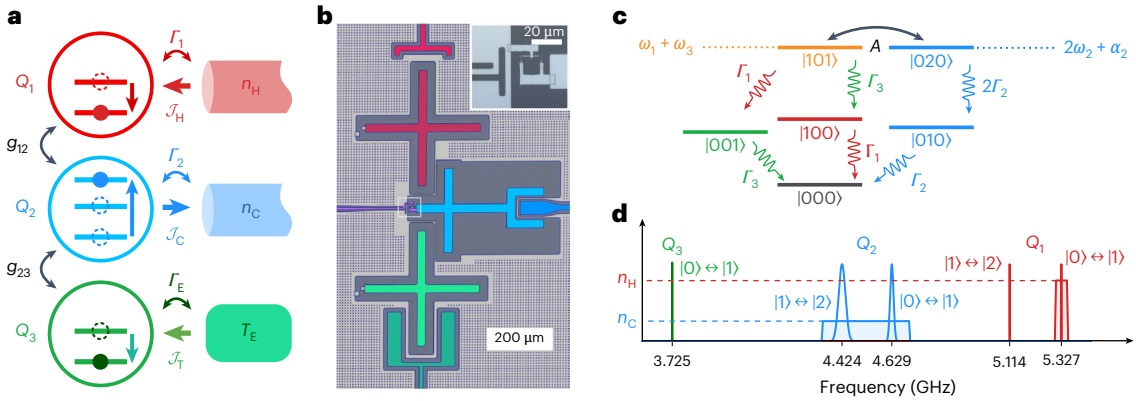

Fig. 1 | Quantum-absorption-refrigerator scheme and level diagram. **a**, Conceptual scheme with three qudits. Qubit Q_1 couples directly to a waveguide at a rate Γ_1; and qudit Q_2, to another waveguide at a rate Γ_2. Qubit Q_3 couples undesirably to an uncontrolled bath in its environment. This bath keeps Q_3 at an effective temperature T_E. The coupling rate Γ_E determines the natural energy-relaxation time of Q_3. The waveguides can operate as heat baths containing photons of average numbers n_H and n_C. The interqudit couplings (g_{12}, g_{23}) engender a process in which one excitation in Q_1 and one excitation in Q_3 are simultaneously exchanged with a double excitation in Q_2. This exchange helps reset Q_3. When heat baths drive this process, the system operates as an autonomous quantum refrigerator. The average heat currents are depicted by wide arrows from the baths of the hot ($\mathcal{J}_H$), cold ($\mathcal{J}_C$) and target ($\mathcal{J}_T$) systems. By energy conservation, $\mathcal{J}_H + \mathcal{J}_T = \mathcal{J}_C$. **b**, False-colour micrograph of the device implemented with superconducting circuits. Q_2 is frequency-tunable due to a flux current line and two parallel Josephson junctions, as magnified in the inset. **c**, Level diagram showing tensor products $|q_1q_2q_3\rangle$ of the qudits' energy eigenstates. $|101\rangle$ and $|020\rangle$ are resonant if $\omega_1 + \omega_3 = 2\omega_2 + \alpha_2$. At resonance, a three-body interaction couples the states at a rate A. **d**, Distributions over the qudits' experimentally observed transition frequencies. The Lorentzian distributions' widths represent spectral widths. The red-shaded box depicts the spectral density n_H of photons injected into the waveguide coupled to Q_1. This synthesized noise realizes the refrigerator's hot thermal bath. Analogous statements concern the blue box, n_C, Q_2 and the cold bath.

temperature of 45–70 mK (refs. 19–22). Furthermore, such passive thermalization takes a few multiples of the qubit's energy-relaxation time—hundreds of microseconds in state-of-the-art setups—delaying the next computation. A quantum machine cooling the qubits to their ground (minimal-entropy) states fulfils criterion (1). Moreover, superconducting qubits inhabit a dilution refrigerator formed from nested plates, whose temperatures decrease from the outermost to the innermost plate. These temperature plates can serve as heat baths, meeting criterion (2). Finally, the machine can retain its quantum nature if mounted on the coldest plate, next to the quantum processing unit, satisfying criterion (3). Such an autonomous machine would be a quantum absorption refrigerator.

Quantum absorption refrigerators have been widely studied theoretically[14,17,23–29]. A previous work[30] reported a landmark proof-of-principle experiment performed with trapped ions. However, the heat baths were emulated with electric fields and lasers, rather than realized with physical heat reservoirs. Other quantum refrigerators, motivated by possible applications, have been proposed[31] and tested[32,33] but are not autonomous.

We report on a quantum absorption refrigerator realized with superconducting circuits. Our quantum refrigerator cools—and therefore resets—a target superconducting qubit autonomously. The target qubit's energy-relaxation time is fully determined by the temperature of the hot bath that we can vary. Using this control, we can vary the energy-relaxation time by a factor of >70. The reset's fidelity is competitive: the target's excited-state population reaches below $3 \times 10^{-4} \pm 2 \times 10^{-4}$ [effective temperatures as low as 22 (+2, −3) mK]. In comparison, state-of-the-art reset protocols achieve populations ranging from 8×10^{-4} to 2×10^{-3} (effective temperatures ranging from 40 mK to 49 mK)[21,22]. Our experiment demonstrates that quantum thermal machines can be not only useful, but also integrated with quantum information-processing units. Furthermore, such a practical autonomous quantum machine expends less control and thermodynamic work than its non-autonomous counterparts[34–36].

Our absorption refrigerator consists of three qudits (d-level quantum systems; Fig. 1a). The auxiliary qudits Q_1 and Q_2 correspond to $d = 2$ and 3, respectively. Each of them couples directly to a waveguide that supports a continuum of electromagnetic modes. The waveguide can serve as a heat bath formed from photons of an arbitrary spectral profile. Here, n_H and n_C denote the average numbers of photons in the waveguides. The target of the refrigerator's cooling is qubit Q_3, which is undesirably coupled to an uncontrolled bath in its environment. This bath excites the target to an effective temperature T_E. Nearest-neighbour qudits couple together with strengths g_{12} and g_{23}. These couplings result in an effective three-body interaction[37], a crucial ingredient in a quantum absorption refrigerator[17,24–26]. We engineer the three-body interaction such that one excitation in Q_1 and one excitation in Q_3 are simultaneously, coherently exchanged with a double excitation in Q_2. Losing its excitation, Q_3 is reset.

As the heat baths drive the resetting, the system operates autonomously as a quantum absorption refrigerator[17]. A generic thermodynamic model describes such a refrigerator as follows. Heat flows from a hot bath (coupled to Q_1) into an intermediate-temperature bath (coupled to Q_2). A heat current of $\mathcal{J}_H$ ($\mathcal{J}_T$) flows out of the bath of Q_1 (Q_3). A net heat current $\mathcal{J}_C = \mathcal{J}_H + \mathcal{J}_T$ enters the bath of Q_2 (Fig. 1a). That is, a temperature gradient, rather than work, coaxes heat out of the target qubit.

The qudits are Al-based superconducting transmons that have Al/AlO_x/Al Josephson junctions[38]. We arrange the qudits spatially in a linear configuration (Fig. 1b). The capacitances between the transmons couple the qudits mutually. Qudit Q_1 has a transition frequency of $\omega_1/(2\pi) = 5.327$ GHz; and qudit Q_2, a variable frequency of $\omega_2/(2\pi)$. Q_1 directly couples capacitively to a microwave waveguide at dissipation rate $\Gamma_1/(2\pi) = 70$ kHz; and Q_2 couples to another waveguide at $\Gamma_2/(2\pi) = 7.2$ MHz. The third qubit, Q_3 has transition frequency $\omega_3/(2\pi) = 3.725$ GHz. Q_3 couples dispersively to a coplanar waveguide resonator. Via the resonator, we read out the state of Q_3 and drive Q_3 coherently. In addition, Q_3 couples to the uncontrolled bath in its environment at a rate Γ_E. In our proof-of-concept demonstration, Q_3 stands for a computational qubit that is being reset and that may participate in a larger processing unit. In the present design, Q_3 has a natural energy-relaxation time $T_{relax} = 1/\Gamma_E = 16.8$ μs, limited largely by Purcell decay into the nearest waveguide, and a residual excited-state population of $P_{res} = 0.028$.

https://doi.org/10.1038/s41567-024-02708-5

The interqudit couplings hybridize the qudit modes. The hybridization, together with the Josephson junctions' nonlinearity, results in a three body interaction (Supplementary Information). For this interaction to be resonant, the qudit frequencies must meet the condition $\omega_1 + \omega_3 = 2\omega_2^{\mathrm{res}} + \alpha_2$. Here, ω_2^{res} denotes the Q_2 frequency that satisfies the equality, and α_2 denotes the anharmonicity of Q_2. The interaction arises from a four-wave-mixing process: one excitation in Q_1 and one excitation in Q_3 are simultaneously exchanged with a double excitation in Q_2 (Fig. 1a)[37]. To satisfy the resonance condition in situ, we make Q_2 frequency-tunable[38]. We control the frequency with a magnetic flux induced by a nearby current line. The device is mounted in a dilution refrigerator that reaches 10 mK.

To describe the resonance condition, we introduce further notation. Let $|0\rangle$ and $|1\rangle$ denote the ground and first excited states of any qudit. Let $|2\rangle$ denote the second excited state of Q_2. We represent a three-qudit state by $|q_1q_2q_3\rangle \coloneqq |q_1\rangle_1 \otimes |q_2\rangle_2 \otimes |q_3\rangle_3$. The resonance condition leads to coherence between the states $|101\rangle$ and $|020\rangle$. This coherence is a key quantum feature of our refrigerator. Two processes, operating in conjunction, reset Q_3. (1) Levels $|101\rangle$ and $|020\rangle$ coherently couple with an effective strength A (Fig. 1c). (2) Q_2 dissipates into its waveguide at a rate Γ_2. The combined action of (1) and (2) brings $|101\rangle$ rapidly to $|010\rangle$ (and then to $|000\rangle$), thereby resetting Q_3.

We engineer the heat baths of Q_1 and Q_2 as follows. First, we synthesize radiation using room-temperature electronics (Supplementary Fig. 1). This radiation has a white-noise spectral profile over a selected frequency range. The radiation is injected into microwave coaxial cables, which are interlinked by dissipative microwave attenuators thermalized at different temperatures of the cryostat. The attenuators reduce the incoming radiation's power and simultaneously introduce quantum thermal noise[39,40]. The last attenuator, at 10 mK, contributes noise that is predominantly quantum vacuum noise. This resulting radiation finally reaches the waveguides of Q_1 and Q_2. Quantum noise is generally characterized by a non-symmetrical spectral density, resulting in different emission and absorption rates of a qudit[41]. Here the predominance of the spontaneous emission of Q_2 into the cold bath (as opposed to absorption) is critical to the refrigerator's operation.

The synthesized radiation's bandwidth is selected to include the transition frequencies of Q_1 ($|0\rangle \leftrightarrow |1\rangle$) and Q_2 ($|0\rangle \leftrightarrow |1\rangle$ and $|1\rangle \leftrightarrow |2\rangle$) (Fig. 1d). Within this bandwidth, the radiation can be approximated as a thermal field. Outside the bandwidth, however, the radiation deviates from thermality. Therefore, we designate this field as quasithermal. Its effective temperature, $T_{\mathrm{H,C}}$, depends on the average number of photons at the transition frequencies of qudits $Q_{1,2}$: $n_{\mathrm{H,C}} = 1/[\exp(\hbar\omega_{1,2}/k_{\mathrm{B}}T_{\mathrm{H,C}}) - 1]$, where k_{B} is Boltzmann's constant. We can vary $n_{\mathrm{H,C}}$ by regulating the synthesized noise's power. This setup enables the whole system to function as a quantum thermal machine. The quasithermal baths induce transitions in Q_1 and Q_2, autonomously driving the reset via the three-body interaction.

Having specified the setup, we demonstrate the three-body interaction. We verify that Q_3 can be reset via resonant driving of Q_1 if and only if Q_2 meets the resonance condition. The qudits begin in $|000\rangle$; accordingly, we issue two microwave drive pulses (Fig. 2a). The first is a Gaussian π pulse that excites Q_3 to state $|1\rangle$: $|000\rangle \rightarrow |001\rangle$.

The second pulse is flat and coherently drives Q_1 (effecting $|001\rangle \leftrightarrow |101\rangle$) at a frequency ω_1^{d} with a rate Ω for a duration Δt. Subsequently, we perform qubit-state readout on Q_3 (we measure $[\langle\sigma_z\rangle + \mathbb{1}]/2$) via the resonator of Q_3.

We investigate the readout's dependencies on ω_1^{d} and on the flux bias voltage (proportional to flux current) that modulates the tunable Q_2 frequency. We have fixed $\Delta t = 2$ μs and $\Omega/(2\pi) = 200$ kHz. The microwave drives that we observe deplete the excited-state population of Q_3 (Fig. 2a). The depletion is the greatest when $\omega_2 = \omega_2^{\mathrm{res}}$ and the drive is resonant ($\omega_1^{\mathrm{d}} = \omega_1$)—when the resonant coupling A between $|101\rangle$ and $|020\rangle$ is the strongest.

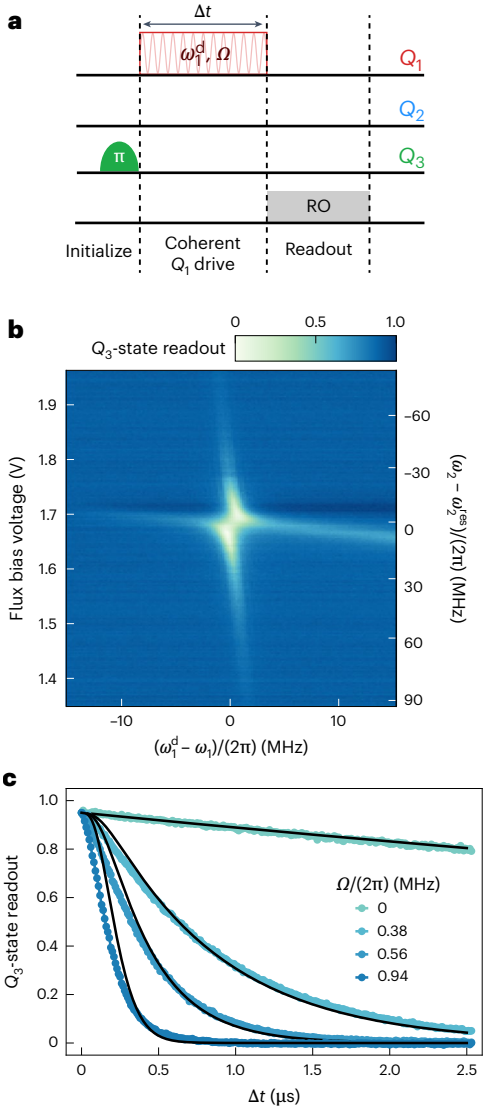

Fig. 2 | Three-body interaction. a, Pulse scheme (see the main text for description). **b**, Two-dimensional plot of the excited-state population of Q_3 ($[\langle\sigma_z\rangle + \mathbb{1}]/2$), as a function of (1) the flux bias voltage (left axis) modulating the frequency of Q_2 and (2) the detuning between the Q_1 drive frequency $\omega_1^{\mathrm{d}}/(2\pi)$ and $\omega_1/(2\pi)$ (bottom axis). Q_1 is driven for $\Delta t = 2$ μs during the pulse scheme, after which we read out (RO) the state of Q_3 via the resonator. The left axis translates directly into the right axis—the detuning of the Q_2 frequency, $\omega_2/(2\pi)$, from the resonant value, $\omega_2^{\mathrm{res}}/(2\pi)$. The white patch evidences an avoided crossing, where $|101\rangle$ and $|020\rangle$ become resonant (Fig. 1c). **c**, Excited-state readout of Q_3 as a function of the duration Δt of the Q_1 drive, at select drive rates $\Omega/(2\pi)$. The solid black lines are fits based on the model shown in Supplementary Section II.

The excited state of Q_3 is depleted by the cascaded processes $|001\rangle \leftrightarrow |101\rangle \leftrightarrow |020\rangle \rightarrow |010\rangle$. The combined effect of these processes resembles optical pumping—used to achieve population inversion in atomic physics—that enables qubit reset. Away from the resonance condition, the resonant coupling A decreases. Consequently, the excited-state population of Q_3 drops less as the $|101\rangle$–$|020\rangle$ detuning grows.

Furthermore, we study the effect of increasing the drive rate Ω (Fig. 2c). When $\Omega = 0$ MHz, Q_3 decays to its ground state (resets) at its natural energy-relaxation time (16.8 μs). As Ω increases, the reset happens increasingly quickly. By fitting a model based on a Lindblad master equation (Supplementary Section II), we determine that the three-body interaction has a strength of $A/(2\pi) = 3.2$ MHz.

https://doi.org/10.1038/s41567-024-02708-5

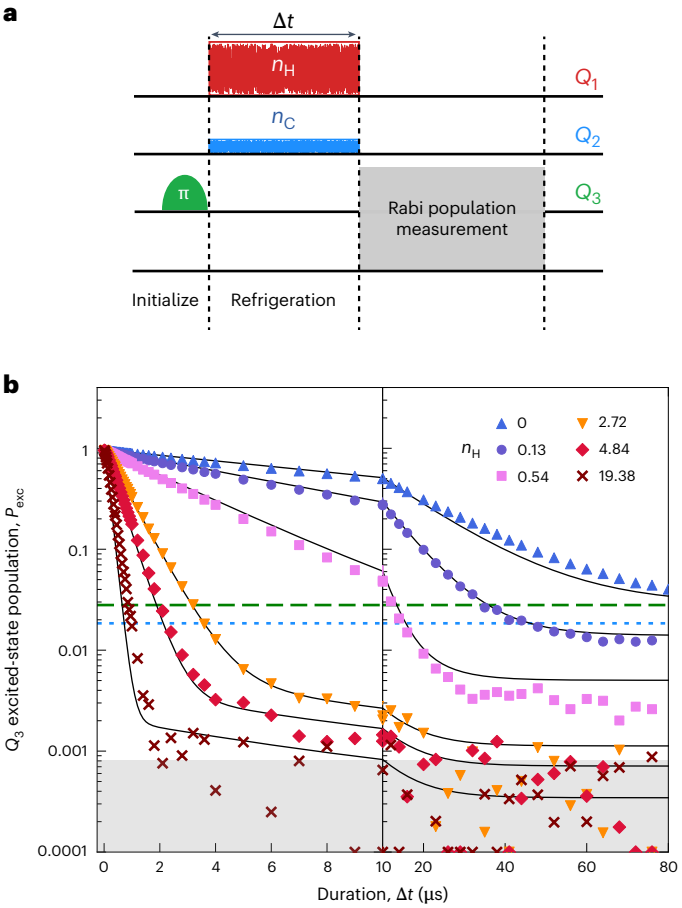

Fig. 3 | Autonomous refrigeration enabled by a hot bath. a, Three-step pulse scheme. Initialization brings the state of Q_3 close to $|1\rangle$. During refrigeration, Q_1 and Q_2 interact with the synthesized quasithermal fields for a duration Δt. Finally, the excited-state population of Q_3, P_{exc}, is measured via a Rabi population-measurement scheme. P_{exc} represents the combined populations of the first and second excited states; the latter is calculated based on a fitted theoretical model and is negligible except at intermediate values of Δt (Supplementary Section III). **b**, P_{exc} as a function of Δt, at select values of n_H, the average number of photons in the hot bath. The x axis is split into two different regimes of Δt values: a low regime $\Delta t \in [0, 10]$ μs and a high regime $\Delta t \in [10, 80]$ μs. Q_2 experiences no synthesized quasithermal field. We estimate that $n_C \approx 0.007$ due to the residual thermal field. The dashed green line shows the residual excited-state population of Q_3 (defined in the main text) as $P_{res} = 0.028$. The dotted blue line shows the excited-state population that Q_3 would have at the cold bath's temperature (45 mK), $P_C = 0.020$. The grey area represents our estimate of the noise floor (Supplementary Section IV). Near the noise floor, some measurements yield small negative values, represented by data points at the bottom axis. The solid lines represent global fits to the experimental curves. The fits are calculated from the model shown in Supplementary Section II. n_H is the sole free-fitting parameter.

Having demonstrated the three-body interaction, we operate the three-qubit system as a quantum thermal machine. To measure the system's performance, we implement a three-step pulse sequence (Fig. 3a). (1) Excite Q_3 to near $|1\rangle$ (to an excited-state population of 0.95). (2) Fill the waveguides with quasithermal photons, as described above, for a variable time interval Δt. (3) Measure the excited-state population of Q_3 (the first two excited states combined), P_{exc}, using a Rabi population-measurement scheme[19,20]. This scheme allows for a more accurate population measurement than standard qubit-state readout. This scheme functions optimally when the second-excited-state population of Q_3 is negligible compared with the first-excited-state population. However, this condition may not always be met when the latter is extremely small ($\lesssim$0.004). Nonetheless, we account for the second-excited-state population of Q_3, determined theoretically from a comprehensively fitted model, in all the population measurements, which are recalibrated accordingly (Supplementary Section III). We assume that the second-excited-state population is exponentially suppressed, arising from the same uncontrolled bath causing the residual first-excited-state population. This recalibration is negligible, except in some narrow subsets of our experimental data, which lie outside the regime in which we evaluate our refrigerator's performance (Fig. 4).

We raise the effective temperature of the hot bath and investigate how P_{exc} responds. To do so, we elevate the average number n_H of quasithermal photons in the hot bath by increasing the spectral power of the synthesized noise in Q_1's waveguide. We perform this study in the absence of synthesized noise in the cold bath (coupled to Q_2), which contains the minimal average number n_C of photons. We infer the minimal n_C from an independent measurement, using Q_2 as a thermometer[40]: $n_C = 0.007$, associated with a temperature $T_C = 45$ mK. The greater the n_H value, the more quickly P_{exc} decays as we increase Δt (Fig. 3b). At the low value $n_H = 0.16$, P_{exc} drops below the residual excited-state population $P_{res} = 0.028$ (Fig. 3b, green dashed line) that Q_3 would achieve if left alone for a long time. From this value, we infer that the effective temperature of Q_3's environment bath $T_E = 50$ mK (Fig. 1a). If thermalized at the cold bath's temperature (45 mK), Q_3 would have an excited-state population of $P_C = 0.020$ (Fig. 3b, blue dotted line). If the hot bath is excited, P_{exc} reaches a value that is at least an order of magnitude lower than P_{res} and P_C. Our refrigeration scheme clearly outperforms passive thermalization with either the intrinsic bath of Q_3 or the coldest bath available. At $n_H = 19.38$ ($T_H = 5.1$ K), refrigeration reduces the effective energy-relaxation time of Q_3, T_{relax}, from 16.8 μs to 230 ns. This reduction is by a factor of >70. Q_3's population declines below 2×10^{-3} over 1.8 μs, before approaching a steady-state value below 0.0008—our measurement protocol's noise floor (Supplementary Section IV).

In an independent measurement, we study the steady-state population P_{SS} as a function of n_H or n_C, keeping the other quantity fixed (Fig. 3a). We define P_{SS} as the P_{exc} value achieved after $\Delta t = 105$ μs. This definition stems from the observation that, when the refrigerator is inactive ($n_H = 0.003$), Q_3 naturally relaxes to its steady-state residual population P_{res} by $\Delta t = 105$ μs. P_{SS} decreases rapidly as n_H increases. Furthermore, P_{SS} reaches its lowest values when n_C minimizes at 0.007, such that Q_2 is not excited. We overestimate the lowest-reached P_{SS} value and its error margin by computing the mean and standard deviation of all the measured P_{SS} values that lie below 0.0008, the noise floor (Supplementary Section IV shows the methodology). P_{SS} reaches a minimum of $<3 \times 10^{-4} \pm 2 \times 10^{-4}$, equivalent to a temperature $T_{SS} = 22(+2, -3)$ mK. This result is remarkably close to the prediction from a general theory of a quantum absorption refrigerator[17]: $T_{SS} = \frac{2\omega_2+\alpha_2-\omega_1}{(2\omega_2+\alpha_2)/T_C-\omega_1/T_H} = 18.6$ mK, equivalent to $P_{SS} = 6.7 \times 10^{-5}$. In the limit as $n_H \to \infty$, T_{SS} decreases marginally to 18.5 mK. T_{SS} does not depend on temperature T_E of the target's effective bath, if Γ_E is very small ($\ll 1/T_{relax}$), as in our system during refrigeration.

Also, raising the cold bath's temperature impedes the reset. Increasing n_C to 0.07—exciting Q_2 more—leads P_{SS} (as a function of n_H) to saturate at a higher value. Finally, consider fixing n_H and increasing n_C. P_{SS} increases rapidly and then saturates near 0.36. This saturation occurs largely independently of n_H. The greater the n_H, though, the greater the initial (low-n_C) P_{SS}.

A standard figure of merit in the thermodynamic analysis of refrigerators is the coefficient of performance (COP)[26]. The COP is to refrigerators as efficiency is to heat engines. The steady-state COP is defined as $\mathcal{J}_T/\mathcal{J}_H$ (Fig. 1a), which we numerically calculate from the theoretical model shown in Supplementary Section II. The steady-state COP is 0.7 when $T_H = 5.1$ K and $T_{SS} = 22$ mK. In terms of COP, our quantum refrigerator performs comparably to a macroscopic absorption

https://doi.org/10.1038/s41567-024-02708-5

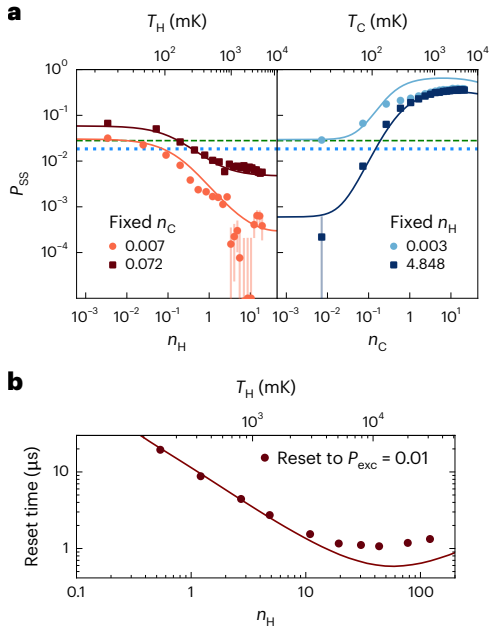

Fig. 4 | Performance metrics of the quantum absorption refrigerator. a, After a 105 μs reset protocol, the excited state of Q_3 reaches a steady-state population P_{SS}. Left: P_{SS} as a function of the hot bath's average photon number, n_H. The corresponding temperature T_H is translated along the top axis. Two experimental curves are at two values of the cold bath's average photon number, n_C. Right: P_{SS} as a function of n_C (translated into temperature T_C on the top axis), at two n_H values. Some measurements yield small negative values, represented by data points at the bottom axis. The dashed green and dotted blue lines are the same as in Fig. 3b. The error bars represent standard deviations about the mean values represented by symbols (Supplementary Section IV). **b**, Reset time (time required for P_{exc} of Q_3 to reach 0.01) as a function of n_H. All the solid lines are theoretical predictions calculated from the model shown in Supplementary Section II.

refrigerator—namely, a common air conditioner [COP ≈ 0.7 (ref. 42)]. In the quasistatic limit (as $\mathcal{J}_T \to 0$), the COP can reach its theoretical upper bound—the Carnot limit: $\frac{T_E(T_H-T_C)}{T_H(T_C-T_E)}$. Our quantum refrigerator has a Carnot bound of 0.95 (>0.7), satisfying the second law of thermodynamics.

Another important performance metric is the time required to reset Q_3. We define the reset time as the time required for P_{exc} to reach 0.01 (corresponding to 38.5 mK). The reset time reaches as low as 970 ns before rising slowly with n_H (Fig. 3b). We attribute the observed upturn to an excessive dephasing of the coherent process $|101\rangle \leftrightarrow |020\rangle$, which is critical for refrigeration.

In summary, we have demonstrated the first quantum thermal machine being deployed to accomplish a useful task. The task—the reset of a superconducting qubit—is crucial to quantum information processing. The machine—a quantum absorption refrigerator formed from superconducting circuits—cools and resets the target qubit to an excited-state population lower than that achieved with state-of-the-art active reset protocols, without requiring external control. Nevertheless, the refrigeration can be turned off when the target qubit serves in a computation: one can either change the hot bath's temperature or detune a qudit out of resonance, using an on-chip magnetic flux.

Our refrigerator has two main quantum features—discrete energy levels and a coherent exchange coupling between states $|101\rangle$ and $|020\rangle$. Another salient feature of our quantum thermal machine is its use of waveguides as physical heat baths. In contrast, other experiments have emulated heat baths[30,35]. Our heat baths consist of quasithermal fields—syntheses of quantum thermal fields and finite-bandwidth artificial microwave noise. Our approach allows control over the baths' temperatures, the ability to tailor spectral properties of the heat baths and the selection of the level transitions to be heated. Thus, this method can facilitate a rigorous study of quantum thermal machines. Our experimental setup can be modified to exploit real-world thermal baths, such as different-temperature plates of a dilution refrigerator. We have already demonstrated that our quantum refrigerator can reset a qubit effectively if it has access to a hot bath at a temperature of a few kelvins, without the need for tuning. Superconducting coaxial cables, together with infrared-blocking filters[43], can expose the qudits to thermal radiation emitted by hot resistors anchored to a suitable plate of the dilution refrigerator[44,45]. The modification adds no significant heat load to the base-temperature plate; nor does it compromise the performance of the quantum information-processing unit. One can activate the thermal reset on demand in two different ways: (1) by using a microwave switch[46] to toggle Q_1's bath between hot and cold or (2) by dynamically detuning Q_2 in and out of the resonance condition that enables the reset process.

Our quantum refrigerator initiates a path towards the experimental studies of quantum thermodynamics with superconducting circuits coupled to propagating thermal microwave fields. Superconducting circuits may also offer an avenue towards scaling quantum thermal machines similarly to quantum information processors. Our experiment may inspire the further development of useful, real-world applications of quantum thermodynamics[47] to quantum information processing[48–50], thermometry[40,45,51], algorithmic cooling[32,52], timekeeping[53] and entanglement generation[54]. This work marks a significant step in quantum thermodynamics towards practical applications.

Online content

Any methods, additional references, Nature Portfolio reporting summaries, source data, extended data, supplementary information, acknowledgements, peer review information; details of author contributions and competing interests; and statements of data and code availability are available at https://doi.org/10.1038/s41567-024-02708-5.

References

1. Horodecki, M. & Oppenheim, J. Fundamental limitations for quantum and nanoscale thermodynamics. *Nat. Commun.* **4**, 2059 (2013).
2. Brandão, F., Horodecki, M., Ng, N., Oppenheim, J. & Wehner, S. The second laws of quantum thermodynamics. *Proc. Natl Acad. Sci. USA* **112**, 3275–3279 (2015).
3. Yunger Halpern, N. & Renes, J. M. Beyond heat baths: generalized resource theories for small-scale thermodynamics. *Phys. Rev. E* **93**, 022126 (2016).
4. Halpern, N. Y. Beyond heat baths II: framework for generalized thermodynamic resource theories. *J. Phys. A* **51**, 094001 (2018).
5. Guryanova, Y., Popescu, S., Short, A. J., Silva, R. & Skrzypczyk, P. Thermodynamics of quantum systems with multiple conserved quantities. *Nat. Commun.* **7**, 12049 (2016).
6. Yunger Halpern, N., Faist, P., Oppenheim, J. & Winter, A. Microcanonical and resource–theoretic derivations of the thermal state of a quantum system with noncommuting charges. *Nat. Commun.* **7**, 12051 (2016).
7. Sparaciari, C., Oppenheim, J. & Fritz, T. Resource theory for work and heat. *Phys. Rev. A* **96**, 052112 (2017).
8. Gour, G., Jennings, D., Buscemi, F., Duan, R. & Marvian, I. Quantum majorization and a complete set of entropic conditions for quantum thermodynamics. *Nat. Commun.* **9**, 5352 (2018).
9. Gelbwaser-Klimovsky, D. et al. Single-atom heat machines enabled by energy quantization. *Phys. Rev. Lett.* **120**, 170601 (2018).
10. Uzdin, R., Levy, A. & Kosloff, R. Equivalence of quantum heat machines, and quantum-thermodynamic signatures. *Phys. Rev. X* **5**, 031044 (2015).

11. Lostaglio, M. Certifying quantum signatures in thermodynamics and metrology via contextuality of quantum linear response. *Phys. Rev. Lett.* **125**, 230603 (2020).
12. Kalaee, A. A. S., Wacker, A. & Potts, P. P. Violating the thermodynamic uncertainty relation in the three-level maser. *Phys. Rev. E* **104**, L012103 (2021).
13. Binder, F. C., Vinjanampathy, S., Modi, K. & Goold, J. Quantacell: powerful charging of quantum batteries. *New J. Phys.* **17**, 075015 (2015).
14. Correa, L. A., Palao, J. P., Alonso, D. & Adesso, G. Quantum-enhanced absorption refrigerators. *Sci. Rep.* **4**, 3949 (2014).
15. Woods, M. P. & Horodecki, M. Autonomous quantum devices: when are they realizable without additional thermodynamic costs? *Phys. Rev. X* **13**, 011016 (2023).
16. Roßnagel, J. et al. A single-atom heat engine. *Science* **352**, 325–329 (2016).
17. Mitchison, M. T. Quantum thermal absorption machines: refrigerators, engines and clocks. *Contemp. Phys.* **60**, 164–187 (2019).
18. DiVincenzo, D. P. The physical implementation of quantum computation. *Fortschr. Phys.* **48**, 771–783 (2000).
19. Geerlings, K. et al. Demonstrating a driven reset protocol for a superconducting qubit. *Phys. Rev. Lett.* **110**, 120501 (2013).
20. Jin, X. Y. et al. Thermal and residual excited-state population in a 3D transmon qubit. *Phys. Rev. Lett.* **114**, 240501 (2015).
21. Magnard, P. et al. Fast and unconditional all-microwave reset of a superconducting qubit. *Phys. Rev. Lett.* **121**, 060502 (2018).
22. Zhou, Y. et al. Rapid and unconditional parametric reset protocol for tunable superconducting qubits. *Nat. Commun.* **12**, 5924 (2021).
23. Palao, J. P., Kosloff, R. & Gordon, J. M. Quantum thermodynamic cooling cycle. *Phys. Rev. E* **64**, 056130 (2001).
24. Linden, N., Popescu, S. & Skrzypczyk, P. How small can thermal machines be? The smallest possible refrigerator. *Phys. Rev. Lett.* **105**, 130401 (2010).
25. Levy, A. & Kosloff, R. Quantum absorption refrigerator. *Phys. Rev. Lett.* **108**, 070604 (2012).
26. Hofer, P. P. et al. Autonomous quantum refrigerator in a circuit QED architecture based on a Josephson junction. *Phys. Rev. B* **94**, 235420 (2016).
27. Nimmrichter, S., Dai, J., Roulet, A. & Scarani, V. Quantum and classical dynamics of a three-mode absorption refrigerator. *Quantum* **1**, 37 (2017).
28. Manikandan, S. K., Jussiau, É. & Jordan, A. N. Autonomous quantum absorption refrigerators. *Phys. Rev. B* **102**, 235427 (2020).
29. Okane, H., Kamimura, S., Kukita, S., Kondo Y. & Matsuzaki, Y. Quantum thermodynamics applied for quantum refrigerators cooling down a qubit. Preprint at https://arxiv.org/abs/2210.02681 (2022).
30. Maslennikov, G. et al. Quantum absorption refrigerator with trapped ions. *Nat. Commun.* **10**, 202 (2019).
31. Manikandan, S. K. & Qvarfort, S. Optimal quantum parametric feedback cooling. *Phys. Rev. A* **107**, 023516 (2023).
32. Baugh, J., Moussa, O., Ryan, C. A., Nayak, A. & Laflamme, R. Experimental implementation of heat-bath algorithmic cooling using solid-state nuclear magnetic resonance. *Nature* **438**, 470–473 (2005).
33. Solfanelli, A., Santini, A. & Campisi, M. Quantum thermodynamic methods to purify a qubit on a quantum processing unit. *AVS Quantum Sci.* **4**, 026802 (2022).
34. Ronzani, A. et al. Tunable photonic heat transport in a quantum heat valve. *Nat. Phys.* **14**, 991–995 (2018).
35. Klatzow, J. et al. Experimental demonstration of quantum effects in the operation of microscopic heat engines. *Phys. Rev. Lett.* **122**, 110601 (2019).
36. Tan, K. Y. et al. Quantum-circuit refrigerator. *Nat. Commun.* **8**, 15189 (2017).
37. Ren, W. et al. Simultaneous excitation of two noninteracting atoms with time–frequency correlated photon pairs in a superconducting circuit. *Phys. Rev. Lett.* **125**, 133601 (2020).
38. Koch, J. et al. Charge-insensitive qubit design derived from the Cooper pair box. *Phys. Rev. A* **76**, 042319 (2007).
39. Caves, C. M. Quantum limits on noise in linear amplifiers. *Phys. Rev. D.* **26**, 1817 (1982).
40. Scigliuzzo, M. et al. Primary thermometry of propagating microwaves in the quantum regime. *Phys. Rev. X* **10**, 041054 (2020).
41. Clerk, A. A., Devoret, M. H., Girvin, S. M., Marquardt, F. & Schoelkopf, R. J. Introduction to quantum noise, measurement, and amplification. *Rev. Mod. Phys.* **82**, 1155 (2010).
42. Welch, T. *Module 10: Absorption Refrigeration* https://www.cibsejournal.com/cpd/modules/2009-11 (2009).
43. Rehammar, R. & Gasparinetti, S. Low-pass filter with ultrawide stopband for quantum computing applications. *IEEE Trans. Microw. Theory Techn.* **71**, 3075–3080 (2023).
44. Goetz, J. et al. Photon statistics of propagating thermal microwaves. *Phys. Rev. Lett.* **118**, 103602 (2017).
45. Wang, Z. et al. Quantum microwave radiometry with a superconducting qubit. *Phys. Rev. Lett.* **126**, 180501 (2021).
46. Pechal, M. et al. Superconducting switch for fast on-chip routing of quantum microwave fields. *Phys. Rev. Appl.* **6**, 024009 (2016).
47. Guzmán, J. A. M., Erker, P., Gasparinetti, S., Huber, M. & Halpern, N. Y. Key issues review: useful autonomous quantum machines. *Rep. Prog. Phys.* https://doi.org/10.1088/1361-6633/ad8803 (2024).
48. Fellous-Asiani, M., Chai, J. H., Whitney, R. S., Auffèves, A. & Ng, H. K. Limitations in quantum computing from resource constraints. *PRX Quantum* **2**, 040335 (2021).
49. Auffèves, A. Quantum technologies need a quantum energy initiative. *PRX Quantum* **3**, 020101 (2022).
50. Aifer, M. & Deffner, S. From quantum speed limits to energy-efficient quantum gates. *New J. Phys.* **24**, 055002 (2022).
51. Mehboudi, M., Sanpera, A. & Correa, L. A. Thermometry in the quantum regime: recent theoretical progress. *J. Phys. A* **52**, 303001 (2019).
52. Alhambra, Á. M., Lostaglio, M. & Perry, C. Heat-bath algorithmic cooling with optimal thermalization strategies. *Quantum* **3**, 188 (2019).
53. Erker, P. et al. Autonomous quantum clocks: does thermodynamics limit our ability to measure time? *Phys. Rev. X* **7**, 031022 (2017).
54. Brask, J. B., Haack, G., Brunner, N. & Huber, M. Autonomous quantum thermal machine for generating steady-state entanglement. *New J. Phys.* **17**, 113029 (2015).

Data availability

Supporting data are available in the figshare data repository (https://doi.org/10.6084/m9.figshare.27089311.v1).

Acknowledgements

This work received support from the Swedish Research Council (M.A.A. and S.G.); the Knut and Alice Wallenberg Foundation through the Wallenberg Center for Quantum Technology (WACQT) (C.C.-M. and S.G.); the European Union, Quantum Flagship project ASPECTS (grant agreement number 101080167) (M.A.A.) and ERC ESQuAT (grant number 101041744) (S.G.); the National Science Foundation, under QLCI grant OMA-2120757 (N.Y.H.) and grant number NSF PHY-1748958 (J.M.E.); the John Templeton Foundation (award number 62422) (J.A.M.G.); and NIST grant number 70NANB21H055 (J.A.M.G.). The studied device was fabricated in Myfab Chalmers, a nanofabrication laboratory.

Author contributions

N.Y.H. and S.G. conceived the experiment. M.A.A., J.A.M.G., J.M.E., N.Y.H. and S.G. performed the theoretical modelling and designed the experiment. M.A.A., P.J.S. and S.G. designed the device. C.C.-M. fabricated the device. M.A.A., P.J.S. and S.G. performed the experiments. M.A.A. and S.G. analysed and interpreted the results. M.A.A., N.Y.H. and S.G. wrote the paper with feedback from P.J.S. and J.A.M.G.

Funding

Open access funding provided by Chalmers University of Technology.

Competing interests

The authors declare no competing interests.

Additional information

Supplementary information The online version contains supplementary material available at https://doi.org/10.1038/s41567-024-02708-5.

Correspondence and requests for materials should be addressed to Mohammed Ali Aamir, Nicole Yunger Halpern or Simone Gasparinetti.

Peer review information *Nature Physics* thanks Machiel Blok and Ruichao Ma for their contribution to the peer review of this work.